



## The Effects of Inclination and Compounds Angles of Round Holes in Staggered Rows on Adiabatic Film Cooling Effectiveness of Vane Suction side

Dr. Najdat N. Abdullah

Department of Mechanical Engineering  
College of Engineering / University of Baghdad  
Email: najdat\_abdulla@yahoo.co.uk

Rashid Khalid Nsaif

Ministry of Oil  
Email: rashidnsaif@gmail.com

### ABSTRACT

The aim of this work is oriented to increase film cooling effectiveness value through numerical investigations for flow of Mach number not more than 0.3 around vane surface, to find the effects of inclination and compounds angles of round holes in staggered rows on adiabatic film cooling effectiveness of vane suction side. Multi cylindrical film cooling hole cases were studied with pitch ratio  $P/d = 2$  and 3, local blowing ratios  $M = 0.382, 0.77$  and 1.14, inclination angles  $\alpha = 30^\circ$  and  $45^\circ$ , compound angles  $\beta = 0^\circ, 15^\circ, 30^\circ$  and  $45^\circ$  and local momentum ratios  $I = 0.084, 0.34$  and 0.756 for better cooling process.

A numerical technique, using ANSYS-FLUENT version 14.5, was used to solve governing partial differential equations of mass, momentum (Navier Stokes equations) and energy conservations in three dimensions with a  $v^2 - f$  turbulence model that involves the solution of the four transport equations. Based on the results of the numerical solution, the best film cooling configuration, blowing ratio, with the range of actual engine flow conditions, dimensions and vane geometry; density ratio 1.74, temperature ratio 0.57 and blowing ratio  $M = 0.382, 0.77$  and 1.14 was obtained. The best case for inclination angle  $\alpha = 30^\circ$ ,  $P/d = 2$  was at  $M = 1.14$  and  $\beta = 0^\circ$  for the total average effectiveness along 60L/d of surface suction side was 0.616, while the best case for inclination angle  $\alpha = 45^\circ$ ,  $P/d = 2$  was at  $M = 0.382$  and  $\beta = 30^\circ$  for the total average effectiveness along 60L/d of surface suction side was 0.516.

In addition, comparisons were performed with available other work, where the experimental total average effectiveness results of Dees et al., 2011 were in good agreements with the numerical results of current work with a maximum deviation of 9.9% at  $I = 0.34$  and 3.6% at  $I = 0.75$ .

**Key words:** vane turbine, film cooling, adiabatic cooling effectiveness.

تأثيرات زوايا الميل والدوران للثقوب الدائرية في الصفوف المتخالفة على كفاءة التبريد الغشائي لجانب السحب من ريش التوجيه الرئيسية في التوربين

راشد خالد نصيف  
وزارة النفط

أ.د. نجدت نشات عبد الله  
كلية الهندسة-جامعة بغداد

### الخلاصة

ان الهدف من هذه الدراسة هو زيادة كفاءة التبريد الغشائي من خلال دراسة نظرية لجريان هواء برقم ماخ لا يزيد عن 0.3 حول سطح الريشة لغرض الوصول الى تأثيرات زوايا الميل والدوران للثقوب الدائرية في الصفوف المتخالفة على كفاءة التبريد الغشائي لجانب السحب من ريش التوجيه الرئيسية في التوربين. تمت دراسة العديد من الحالات نظريا لثقوب تبريد اسطوانية بنسبة مسافة بين ثقبين الى قطر الثقب هي 2 و 3 وبمعدل ضخ نسبة الى السرعة الموقعية للجريان الرئيسي هو 0.328 و

0.77 و 1.14 و بزواوية توجيه علوي 30° و 45° وزاوية توجيه جانبي 0°, 15°, 30°, 45° وبعزم ضخ 0.084, 0.34, 0.756 لافضل تبريد.

باستخدام الحل العددي بواسطة البرنامج ANSYS-FLUENT version 14.5 تم حل المعادلات التفاضلية الجزئية بالاتجاهات الثلاثة للكتلة والعزم والمعروفه Navier Stokes equations بالاضافة لمعادلة الطاقة وباستخدام نموذج  $v^2 - f$  للجريان المضطرب الذي يشمل اربع معادلات انتقال. بالاعتماد على نتائج الحل العددي والتي هي بظروف مشابهة لظروف المحرك التوربيني من الناحية النسبية نسبة كثافة 1.74، نسبة درجات حرارة 0.57، نسبة ضخ 0.382, 0.77, 1.14، تم الوصول الى أمثل: شكل وكمية الضخ. الحالة الامثل عندما تكون زاوية الميل  $\alpha=30^\circ$ ،  $P/d=2$ ، هو عند  $\beta=0^\circ$  and  $M=1.14$  حيث المعدل الكلي لكفاءة التبريد لطول 60L/d من سطح السحب لريشة التوربين هو 0.616، بينما الحالة الامثل عندما تكون زاوية الميل  $\alpha=45^\circ$ ،  $P/d=2$ ، هو عند  $\beta=30^\circ$  and  $M=0.382$  حيث المعدل الكلي لكفاءة التبريد لطول 60L/d من سطح السحب لريشة التوربين هو 0.516.

تمت المقارنة مع بحوث متوفرة لاعمال أخرى حيث كانت النتائج العملية لمعدل التبريد الكلي للباحث Dees et al., 2011 متقاربة بشكل جيد مع النتائج العملية لهذه الدراسة وكانت اعلى نسبة للاختلاف بين العمليين هو 9.9% عند نسبة عزم للضخ 0.34 و 3.6% عند نسبة عزم ضخ 0.75. الكلمات الرئيسية: ريش التوربين، التبريد الغشائي، الكفاءة التبريد الاديابتيكي.

## 1. INTRODUCTION

Modern high pressure turbine blade and vane are set under high thermal stress. Since the early years, the turbine combustion gases inlet temperature has been increasing considerably in order to increase the work output per unit mass and the thermal efficiency of gas turbine engine. Nowadays, the combustion gases temperature in the first stages of turbine can be beyond acceptable vane metal temperatures. In order to keep vanes at an acceptable temperature, a complex cooling ways were used. Many works were made in the earlier years in order to increase the cooling efficiency and in the recent years continuous efforts are doing to develop the technologies for higher blade loading, **Gomes and Niehuis, 2013 part II**. Film cooling technique is widely used for the vanes and blades of the front stages in order to reduce material temperatures as far as necessary for an acceptable life span of the components. As film cooling jets reduced combustion gases temperature, improvements can be gain by decreasing the amount of jet cooling mass flow rate and with effective film cooling distribution on vane surface, **Kusterer, et al., 2007**.

Several global researches studied the vane film cooling and great affords was done to improve film cooling method. **Cutbirth and Bogard, 2002**, defined thermal fields of the showerhead film cooling region which is part of suction side of a turbine vane by using a closed-loop, low speed wind tunnel with ranged of blowing ratios from 0.5 to 2.0. Showerhead cooling jet was completely lift-off from the vane surface even at low blowing ratios and the interaction of the coolant jets from lateral adjacent holes improve adiabatic film cooling effectiveness. **Dittmar, et al., 2003**, investigated four different film-cooling hole configurations on a large scale suction side of vane in open loop atmospheric wind tunnel and one of them was staggered arrangement of double row cylindrical holes. It was found that all configurations show similar film-cooling effectiveness at low blowing ratios. Effectiveness was decreased drastically for the cylindrical holes which were attributed to coolant jet separation from the vane surface. **Colban, et al., 2006**, presented a study of the adiabatic cooling effectiveness and heat transfer coefficients for turbine vane under low-speed conditions by using low speed wind tunnel. Near the leading edge, the Stanton number had the maximum value. Measurements of single row adiabatic film cooling effectiveness without upstream showerhead blowing showed that the jet lift-off was along vane suction side. **Waye and Bogard, 2007**, investigated adiabatic film cooling effectiveness for round axial hole and with compound angle on

the simulated vane suction side to evaluate the performance of these configurations. Experiments were conducted by using low speed wind tunnel for different coolant density ratio, main flow turbulence levels, and hole spacing. Compound angle holes provided higher laterally averaged adiabatic effectiveness than axial holes and the adiabatic effectiveness for the compound angles, showed better than axial holes. **Dees, et al., 2011**, presented experimental measurements of external surface temperature on the cooled adiabatic model of scaled up vane suction side. Adiabatic effectiveness values were measured on downstream of the film cooling holes near the mid span of adiabatic vane at local momentum ratio  $I = 0.34$  and  $0.75$ . The highest values of laterally averaged adiabatic effectiveness occur immediately downstream of film injection. At  $I = 0.34$  best effectiveness was obtained over the whole test domain. Increasing the film cooling momentum flux ratio decreased the adiabatic effectiveness values due to coolant flow separation.

**Mhetras, et al., 2012**, studied experimentally the effect of cooling holes location in lateral direction of a stationary linear cascade on film-cooling effectiveness using the pressure sensitive paint method. The effect of showerhead cooling jet at vane leading edge and the compound angle hole type on the suction sides were examined. **Dyson, et al., 2013**, measured the adiabatic and overall effectiveness for a scaled up linear vane cascade model, fully cooled, with film cooling holes on a showerhead and rows on vane suction side in a low speed wind tunnel with a “chord-exit Reynolds number” of 700,000. Adiabatic effectiveness measured for a model was constructed from foam low thermal conductivity. The spatial variation in the overall effectiveness was considerably less than that for the adiabatic effectiveness. **Naik, et al., 2014**, investigated film cooling effectiveness characteristics of a first stage turbine via numerical method. The oil flow visualization indicated that the secondary flows on the vane suction side were relatively small. The impact of high and low blowing ratios was relatively small on the film cooling effectiveness.

A model studied in this work represents the actual dimensions of vane geometry of 125MW gas turbine for South Baghdad Power Station as given in **Table 1**. Study of performance of gas turbine vane suction side film cooling effectiveness was investigated through different inclination and orientation angles of film cooling holes. Multi cylindrical film cooling holes cases were studied as shown in **Table 2** to find the best case for better cooling.

## 2. NUMERICAL SOLUTION

In order to analyze the fluid flow and heat transfer characteristics mathematically at vane suction sides of turbine, a solution of Navier-Stokes equations is required. Due to the complexity of vane surface configuration and the significant viscous and heat effects, it is impossible to obtain an analytical solution of Navier-Stokes equation. Therefore, a numerical technique, using ANSYS-FLUENT version 14.5, was used to solve governing partial differential equations of mass, momentum and energy conservations in three dimensions with a  $v^2 - f$  turbulence model that involves the solution of the four transport equations; the turbulence kinetic energy  $k$ , its rate of dissipation  $\epsilon$ , the velocity variance scale  $\overline{v^2}$  and the elliptic relaxation function  $f$ , to demonstrate the effect of the turbulence on the flow structure.

The annular geometry of vanes was converted to straight for one vane with periodic boundary condition from suction and pressure side and symmetry boundary conditions in span direction far from endwall effects at the hub and shroud as shown in **Fig. 1**. Only 12mm in the middle of the span which contains holes film cooling, was modeled. This method was used by, **Colban, et al., 2007**.

For the modeled geometry, the distance from inlet section of combustion gases to the leading edge of the vane is 55mm, while the distance from vane trailing edge to exit boundary of combustion gases is 30mm and the distance between periodic boundaries was 167mm and all other dimensions are listed in **Table 1**. Depending on the dimensions of actual vane gas turbine for South Baghdad Power Station 125MW, the same dimensions of cylindrical film cooling holes have been made in a model vane with different inclination and compound angles in order to investigate its effects on adiabatic film cooling effectiveness on vane suction side. In this work, air was chosen as a working fluid and cold air was used in film cooling flow while the hot air represents the hot main stream flow. The physical properties for stream was fed as an input to ANSYS-FLUENT and used in solving the cases.

Pointwise V17.0R1 was used to generate structured, unstructured and hybrid grids. Structured grid was used around the vane surface for a sufficient distance from the vane surface and then completed the whole domain by using unstructured grid which result a hybrid mesh in the block that a mixture from hexahedron, pyramid and prism cells as shown in **Fig. 1**. Non-conformal grids was produced due to the difference in cells configuration between vane wall cells and cooling hole exit area cells (named interface where the locations of grid node at the meet boundaries of two subdomains not identical).

To obtain accurate solution in this work, skewness kept to not exceed 0.85 for hex, quadratic and triangular cells and for tetragonal cells, skewness should not exceed 0.9. The mesh adjacent to the wall was so fine to solve the boundary layer flow. In the film cooling researches that presented, the recommended value of  $y^+$  is less than four. In this work the value of  $y^+$  near the vane surface was kept at a value  $y^+ = 1$ .

For structured domains the orthogonality of grid points adjacent to the vane wall was kept to perfect orthogonality and max value was  $90^\circ$  along the entire vane surface. For the present model 1,091,160 cells was used. The rate of convergence is indication to mesh quality. In this work the convergence was achieved with about 160 iterations.

The numerical study of this work depends on the general gas turbine engine conditions that was specified and used from a very few researches as was found in the literature surveyed. These engine conditions represented by density ratio  $DR=1.2$  to  $1.75$ , temperature ratio  $\frac{T_c}{T_\infty} = 0.5$  to  $0.7$  and blowing ratio  $M=0.3$  to  $1.5$ . In this research will focus on the effect of inclination and compound angle of round hole on adiabatic film cooling effectiveness for  $P/d=2$  on vane suction side.

The free stream out from the combustion chamber is normally turbulent or the simulation one in this study entering the vane inlet boundary and flowing around the vane surfaces suction and pressure side. This flow is as a flow around an obstacle and it considered as external flow **Mathew, et al., 2013**. Flow around obstacle was considered as turbulent for  $Re_d \geq 20,000$ . The Reynolds number for the model vane is  $Re_d = 25100$  where the characteristic length is the leading edge diameter. The characteristic Reynolds number depending on vane cord length as a characteristic length is normally high  $Re_c = 1.49E+05$  in this study depending at inlet velocity and  $Re_c = 5.51E+05$  depending on exit velocity at trailing edge and 20% turbulent intensity was used at free stream inlet velocity.

In the present work, the working fluid was air and the flow characteristics were assumed to be three-dimensional turbulent incompressible Newtonian fluid flow, density  $\rho$  varies only with



temperature and single-phase flow. In addition, flows pressure work  $\frac{P}{\rho}$ , and kinetic energy  $\frac{v^2}{2}$  terms in energy equation are negligible, viscous dissipation terms  $(\bar{\tau}_{eff} \cdot \vec{V})$  are negligible and  $S_h = 0$ .

In this work Reynolds averaged Navier-Stokes equations RANS was used, **ANSYS theory guide, 2014**.

In Cartesian tensor, they can be written as:

$$\frac{\partial \rho \bar{u}_i}{\partial x_i} = 0 \quad (1)$$

$$\frac{\partial}{\partial x_j} \rho \bar{u}_i \bar{u}_j = -\frac{\partial \bar{P}}{\partial x_i} + \frac{\partial}{\partial x_j} \left[ \mu \left( \frac{\partial \bar{u}_i}{\partial x_j} + \frac{\partial \bar{u}_j}{\partial x_i} - \frac{2}{3} \delta_{ij} \frac{\partial \bar{u}_i}{\partial x_i} \right) \right] \quad (2)$$

where  $(-\rho \bar{u}_i \bar{u}_j)$  is a Reynolds stress tensor  $R_{ij}$  which represents the effects of turbulence. The forma of energy equation that solves in ANSYS FLUENT, was:

$$\nabla \cdot \vec{V} \rho E + P = \nabla \cdot \left( k_{eff} \nabla T - \sum_j h_j \vec{j}_j + (\bar{\tau}_{eff} \cdot \vec{V}) \right) + S_{\bar{h}} \quad (3)$$

The film cooling flow over the vane surface is a boundary layer flow. The most suitable turbulent model for this type of flow considering the boundary layer is  $v^2 - f$  model. This model is the successful modeling of the separation of fluid from a curved surface for example, the suction side of an airfoil. The turbulence kinetic energy  $k$ , rate of dissipation  $\varepsilon$ , the velocity variance scale  $\overline{v^2}$ , and the elliptic relaxation function  $f$  can be obtained from the following transport equations:

$$\frac{\partial}{\partial x_i} (\rho k \bar{u}_i) = P_k - \rho \varepsilon + \frac{\partial}{\partial x_j} \left[ \left( \mu + \frac{\mu_t}{\sigma_k} \right) \frac{\partial k}{\partial x_j} \right] \quad (4)$$

$$\frac{\partial}{\partial x_i} (\rho \varepsilon \bar{u}_i) = \frac{C_{\varepsilon 1} P_k - C_{\varepsilon 2} \rho \varepsilon}{T} + \frac{\partial}{\partial x_j} \left[ \left( \mu + \frac{\mu_t}{\sigma_\varepsilon} \right) \frac{\partial \varepsilon}{\partial x_j} \right] \quad (5)$$

$$\frac{\partial}{\partial x_i} (\rho \overline{v^2} \bar{u}_i) = \rho k f - 6 \rho \overline{v^2} \frac{\varepsilon}{k} + \frac{\partial}{\partial x_j} \left[ \left( \mu + \frac{\mu_t}{\sigma_k} \right) \frac{\partial \overline{v^2}}{\partial x_j} \right] \quad (6)$$

$$f - L^2 \frac{\partial^2 f}{\partial x_j^2} = (C_1 - 1) \frac{2}{3} \frac{\overline{v^2}}{k} + C_2 \frac{P_k}{\rho k} + \frac{5 \overline{v^2}}{T} \quad (7)$$

The model constants have the following default values:

$\alpha = 0.6$ ,  $C_1 = 1.4$ ,  $C_2 = 0.3$ ,  $C_{\varepsilon 1} = 1.4$ ,  $C_{\varepsilon 2} = 1.9$ ,  $(C_\eta = 70)$ ,  $C_\mu = 0.22$ ,  $C_L = 0.23$ ,  $\sigma_k = 1$ ,

$\sigma_L = 1.3$ ,  $\hat{C}_{\varepsilon 1} = C_{\varepsilon 1} \left( 1 + 0.045 \sqrt{k / \overline{v^2}} \right)$ , **ANSYS Fluent  $v^2 - f$  turbulence model manual, 2013**.

Boundary conditions were specified for each zone of the computation domain. For the steady state, there were four boundaries in the physical flow domain, inlet, outlet, periodic boundary and solid surfaces wall as shown in **Fig. 1**. However, the internal domain zone that shares common areas faces does not require any boundary condition.

The boundary conditions used in this work are as follow:

- Velocity-inlet boundary at area NO.1, where  $U_\infty = 23\text{m/s}$ ,  $T_\infty = 527\text{k}$ ,  $T_u = 20\%$ ,  $D_h = 22.3\text{mm}$  and pressure gage=0.
- Pressure outlet boundary at area NO.2, where  $T_\infty = 527\text{k}$ ,  $T_u = 5\%$ ,  $D_h = 22.3\text{mm}$ .
- Periodic boundary at area NO.3.
- Velocity-inlet boundary at area NO.4, where its velocity depend on blowing ratios with  $T_\infty = 300\text{k}$ ,  $D_h = 2\text{mm}$ .
- Symmetry boundary at area NO.5
- Wall boundary at area NO.6, no-slip and adiabatic wall was defining by setting a zero heat flux condition.
- Zero-gradient boundary condition for the variable  $f$  at inlets with default value = 1
- $k$ ,  $\varepsilon$ ,  $\sqrt{v^2}$  and  $\ell$  at inlet boundaries were compute its initial values from:

$$k = 1.5(T_u U_\infty)^2 \quad ; \quad \varepsilon = 0.09^{0.75} \frac{k^{3/2}}{\ell} \quad ; \quad \sqrt{v^2} = \frac{2}{3}k \quad ; \quad \ell = 0.07(D_{h \text{ of area 1 or 4}})$$

**ANSYS Fluent  $v^2 - f$  turbulence model manual, 2013.**

In this work the predicting near-vane wall cell distance was specified according to  $y^+ = 1$ , a good power law correlation for a flat plate for turbulent coefficient of skin friction was used, **Saadati, 2009**, as follows:

$$C_f \approx 0.027 Re_x^{1/7} \quad (8)$$

Wall shear stress was predicted from;

$$\tau_w = \frac{1}{2} C_f \rho U_\infty^2 \quad (9)$$

From  $\tau_w$  compute the velocity  $U_\tau$ ;

$$U_\tau = \sqrt{\frac{\tau_w}{\rho}} \quad (10)$$

The distance from the wall to the centroid of the first cell  $\Delta y$  can be estimated by choosing the desired wall distance vector  $y^+ = \frac{y U_\tau}{\nu}$  dimensionless where  $y$  distance from the wall.

$$\Delta y = \frac{y^+ \mu}{U_\tau \rho} \quad (11)$$

To characterize the film cooling performance, adiabatic film cooling effectiveness was used. It represent a normalized form of  $T_{aw}$  (the coolant temperature at the wall will be at the adiabatic wall temperature,  $T_{aw}$ , which it was the driving temperature potential for heat transfer into the wall). The film effectiveness  $\eta$  is defined as follows, **Bogard, 2012**:

$$\eta = \frac{T_\infty - T_{aw}}{T_\infty - T_{c,exit}} \quad (12)$$

In this work Mach number (Ma) is assumed to not exceed 0.3 in two passages around the vane surface, in order to be within incompressible flow range. The velocity was kept approximately at  $U_{\infty} = 23 \text{ m/s}$  at the inlet of vane near the leading edge to ensure the Mach number not exceeds 0.3 around the vane. This velocity was specified via using Auto-Cad program and thus the minimum vane passage flow area was calculated (it is equal to  $0.0003396 \text{ m}^2$ ). Also, the cross sectional area between two stagnation points on the pair of the neighbor vanes was equal to  $0.002 \text{ m}^2$ . The velocity of sound ( $a$ ) at the temperature of hot main stream flow of  $527\text{C}^{\circ}$  was equal to  $458 \text{ m/s}$  that found from Eq. (13).

$$a = \left(\frac{C_p}{C_v}\right) R T)^{0.5} \quad (13)$$

$$U = Ma * a \quad (14)$$

Hence, from Eq. (14), the maximum hot flow speeds at minimum vane passage cross section area was computed.

#### 4. RESULTS AND DISCUSSIONS

As shown from the contours of vane static temperature, **Fig. 2**, the staggered arrangement of holes improves the film cooling on vane surface where the upstream row of staggered arrangement fills the film cooling gap between the holes of downstream row of staggered arrangement. As shown in the jet film cooling fully attached to vane surface because of low momentum ratio  $I=0.085$  corresponding to blowing ratio of  $M=0.382$ . The local span average effectiveness of case (1) for  $\beta=0^{\circ}$ ,  $15^{\circ}$  and  $30^{\circ}$  along  $60L/d$  was presented in **Fig. 3** with insignificant difference among local span effectiveness. The values of total average effectiveness for these cases were 0.342, 0.413 and 0.387 respectively. **Figure 4** shows local span average effectiveness for case (2) for  $\beta=0^{\circ}$ ,  $15^{\circ}$  and  $30^{\circ}$  along  $60L/d$  of vane surface distance. At  $\beta=30^{\circ}$ , the cooling jet was lift-off little from the hole trailing edge of the downstream row and reattached at  $8L/d$  after mixes with hot gases and the temperature of cooling jet was increased. While the cooling jets for  $\beta=0^{\circ}$  and  $15^{\circ}$  were fully attached to the vane surface which that improve the cooling effectiveness. The momentum ratio of  $I=0.34$  corresponds to  $M=0.77$  was the moderate between  $I=0.25$  and  $I=0.5$ . Below  $I=0.25$  the cooling jet was fully attached the vane surface and for  $I=0.5$  and above the cooling jet flow was separated. The value of total average effectiveness at  $60L/d$  surface distance was 0.517, 0.535 and 0.432 respectively. The local span average effectiveness of case (3) for  $\beta=0^{\circ}$ ,  $15^{\circ}$  and  $30^{\circ}$  along  $60L/d$  was presented in **Fig. 5**. The cooling jet was fully attached the vane surface at  $\beta=0^{\circ}$  and  $15^{\circ}$ . For  $\beta=30^{\circ}$ , the jet was separated and mixed with hot mainstream gas that flows above the cooling jet and between the gap formed in cooling jet from staggered holes arrangement and the second vortex system of hot gas sweeps and mixes under cooling jet and warm the gap area and the cooling jet warms and mixes as it flows in downstream direction. The value of total average effectiveness at  $60L/d$  surface distance was 0.616, 0.496 and 0.366 respectively.

Among the cases (1, 2 and 3) the best one that gave higher total average effectiveness along  $60L/d$  was case (3) at  $\beta=0^{\circ}$  ( $\eta=0.616$ ) where the local span average effectiveness for this case as shown in **Fig.6**. It was obvious that the case 3 at  $\beta=0^{\circ}$  had the highest total average effectiveness of 0.616, but for the case 2 at  $\beta=15^{\circ}$  had also a good value of total average effectiveness 0.535. The

percentage difference between two values of total average effectiveness was 8.1% and this value was achieved by increasing the blowing ratio from 0.77 to 1.14 which represents 25.2%.

**Fig. 7** represents the span average effectiveness of case 4 for  $\beta=0^\circ, 15^\circ, 30^\circ,$  and  $45^\circ$ . In this case, the cooling jet fully attached to vane surface. While the high inclination angle,  $\alpha=45^\circ$  assists the jet to separate, but the low blowing ratio  $M=0.382$  and its corresponding low momentum ratio prevent the separation. Due to low blowing ratio, the cooling jet quickly losses its coldness due to mixing with hot flow stream. This mix is proportional with degree of compound angle.  $\beta=30^\circ$  produces a high lateral cooling distribution and increases perfectly the effectiveness. The values of total average effectiveness along 60L/d of vane surface were 0.375, 0.362, 0.516 and 0.334 respectively. **Fig. 8** shows the span average effectiveness of case (5) for  $\beta=0^\circ, 15^\circ, 30^\circ,$  and  $45^\circ$ . At  $\beta=0$  and  $15^\circ$ , the cooling jet attached to the surface with not allowing the hot gases to control and weaken the cooling effect. For  $\beta=30^\circ$ , lift-off was occurred and reattached at 5L/d while at  $\beta=45^\circ$  lift off was occurred and mixed with hot gases and causes poor in lateral cooling distribution which decreases the cooling effectiveness. Very good lateral cooling distribution at compound angle  $15^\circ$  and  $30^\circ$ . The values of total average effectiveness for  $\beta=0^\circ, 15^\circ, 30^\circ,$  and  $45^\circ$  were 0.47, 0.523, 0.487 and 0.215 respectively. From **Fig. 9** the span average effectiveness of case (6) for  $\beta=0^\circ, 15^\circ, 30^\circ,$  and  $45^\circ$  were clarified. At  $\beta=0^\circ$  and  $15^\circ$  the hot gas don't mix strongly with cooling jet and the cold mixture still in touch with the vane surface with good lateral cooling distribution. At  $\beta=30^\circ$  the cooling jet were separated and warmed via mixes with hot gas and reattached at 6L/d after losing some of its cooling effect with few lateral distributions. At  $\beta=45^\circ$  the cooling jets mixed with hot gas, converged and lost the cooling effect after 8L/d. The values of total average effectiveness for  $\beta=0^\circ, 15^\circ, 30^\circ,$  and  $45^\circ$  were 0.524, 0.452, 0.286 and 0.09 respectively. Among cases (4, 5 and 6) the best one that gave higher total average effectiveness along 60L/d was case 6 at  $\beta=0^\circ$  ( $\eta=0.524$ ). It was clear that the values of total average effectiveness of these three cases had the highest and approximately equal values which were 0.516 at  $\beta=30^\circ, 0.523$  at  $\beta=0^\circ,$  and  $0.524$  at  $\beta=0^\circ,$  respectively. The choosing one of these values as the best case must not depend on the highest value of total average effectiveness only, but also depends on the blowing ratio for each of these cases must. The increase of blowing ratio from 0.382 to 1.14 represents 50.8% increasing in blowing ratio which reduces gas turbine engine efficiency. The percentage increase in total average effectiveness from 0.523 to 0.524 was 0.1% with corresponding to percentage increase in blowing ratio 25.2% for increasing  $M$  from 0.77 to 1.14. So that the case (6) with  $\beta=0^\circ$  will be out of the interest. Thus the comparison will be between case 4 at  $\beta=30^\circ,$  and case (5) at  $\beta=0^\circ$ . The percentage increase in total average effectiveness for these cases, from 0.516 to 0.523 is 0.7% with corresponding increasing in blowing ratio of 25.6% for increasing  $M$  from 0.382 to 0.77. So that the best case was case (4) at  $\beta=30^\circ,$  because it was not logic to cool and increase the gas turbine efficiency of 0.7% by increasing the injection cooling air through increase blowing ratio 25.6% .

The best case for thirty degrees inclination angles of film cooling holes was the case (3) at  $\beta=0^\circ$  that had the value of 0.616 total average effectiveness, and the best case for forty five degrees inclination angle of film cooling holes was the case (4) at  $\beta=30^\circ,$  that had the value of 0.516 total average effectiveness. The difference between the values of total average effectiveness 0.616 and 0.516 is 10%. This 10% increase accomplished with increase in blowing ratio of 50.8% .The designer of gas turbine engine is the only person has the permission to decide whether this 10% increase in cooling effectiveness worth to increase blowing ratio. In this work the case (3) at  $\beta=0^\circ$



with total average effectiveness 0.616 was chosen to be the best case among all the twenty one different cases as shown in **Fig. 10**.

Comparison was made between cases from current work and experimental cases from **Dees, et al., 2011**, as shown in **Fig. 11**. Two cases from current study on the vane suction side, consists of a line of holes at  $\alpha=45^\circ$ ,  $\beta=0^\circ$ ,  $P/d=3$  at  $I=0.75$  and the second at  $I=0.34$ . These two cases were compared with two cases from **Dees, et al., 2011**, work with a line of holes at the suction side of scaled up vane four times bigger than the actual size at  $\alpha=42^\circ$ ,  $\beta=0^\circ$ ,  $P/d=3$ , where first case at  $I=0.75$  and the second at  $I=0.34$ . It was obvious that the value of local momentum factor was close together among the compared cases. It was obvious that there were no lift-off occurred in the cooling jet for both cases of **Dees et al., 2011**, while in current study, the cooling jet lift-off was found and reattached at  $5.4L/d$ . So that the total average effectiveness of **Dees, et al., 2011** two cases was 0.279 at  $I=0.34$  and 0.206 at  $I=0.75$  along  $55L/d$  where higher than the total average effectiveness of current cases, which were 0.18 at  $I=0.34$  and 0.17 at  $I=0.75$ . The reason of these differences in cooling performance between cases of **Dees, et al., 2011**, and current study cases were related to used actual engine vane size in this work, while **Dees, et al., 2011**, was used scaled up four times larger than the actual engine vane size. Generally, for  $I=0.34$  and  $I=0.75$  for current study as shown in **Fig. 11** was closed to spouse results of **Dees, et al., 2011**, cases especially after  $16L/d$ , where the maximum deviation of 9.9% at  $I=0.34$  and 3.6% at  $I=0.75$ .

## 5. CONCLUSIONS

The following conclusions were extracted from numerical simulation results on the prediction of the best configurations of film cooling round holes on vane suction side:

- 1- For case (1) the highest effectiveness was at  $\beta=15^\circ$  with the total average effectiveness along  $60L/d$  was 0.413.
- 2- For case (2) the highest effectiveness was at  $\beta=15^\circ$  with the total average effectiveness along  $60L/d$  was 0.535.
- 3- For case (3) the highest effectiveness was at  $\beta=0^\circ$  with the total average effectiveness along  $60L/d$  was 0.616.
- 4- For case (4) the highest effectiveness was at  $\beta=30^\circ$  with the total average effectiveness along  $60L/d$  was 0.516.
- 5- For case (5) the highest effectiveness was at  $\beta=0^\circ$  with the total average effectiveness along  $60L/d$  was 0.523.
- 6- For case (6) the highest effectiveness was at  $\beta=0^\circ$  with the total average effectiveness along  $60L/d$  was 0.524.
- 7- The best case for inclination angle  $\alpha=30^\circ$  was case (3) at  $\beta=0^\circ$  with the total average effectiveness along  $60L/d$  of surface suction side was 0.616, while the best case for inclination angle  $\alpha=45^\circ$  was case (4) at  $\beta=30^\circ$  with the total average effectiveness along  $60L/d$  of surface suction side was 0.516.

## REFERENCES

- ANSYS Fluent 12.1, 2012, *Using Flow Boundary Conditions*.
- ANSYS Fluent, 2013,  *$v^2 - f$  Turbulence Model Manual*.



- ANSYS Fluent, 2014, *Theory Guide*.
- Bogard, D. G., 2012, *Airfoil Film Cooling*, web site: <https://www.netl.doe.gov>.
- Colban, W., Gratton, A., Thole, K. A., and Haendler, M., 2006, *Heat Transfer and Film-Cooling Measurements on a Stator Vane with Fan-Shaped Cooling Holes*, ASME J. Turbomach., Vol. 128.
- Colban, W., Thole, K. A., and Haendler, M. 2007, *Experimental and Computational Comparisons of Fan-Shaped Film Cooling on A Turbine Vane Surface*, ASME J. Turbomach., Vol. 129.
- Cutbirth, J. M., and Bogard, D., 2002, *Thermal Field and Flow Visualization within the Stagnation Region of a Film-Cooled Turbine Vane*, ASME J. Turbomach., Vol. 124.
- Dees, J. E., Bogard, D. G., Ledezma, G. A., and Laskowski, G. M., 2011, *Overall and Adiabatic Effectiveness Values on a Scaled Up, Simulated Gas Turbine Vane: Part I – Experimental Measurements*, ASME paper GT2011-46612.
- Dittmar, J., Schulz, A., and Wittig, S., 2003, *Assessment of Various Film-Cooling Configurations Including Shaped and Compound Angle Holes Based on Large-Scale Experiments*, ASME J. Turbomach., Vol. 125.
- Dyson, T. E., McClintic, J. W., Bogard, D. G., and Bradshaw, S. D., 2013, *Adiabatic and Overall Effectiveness for a Fully Cooled Turbine Vane*, ASME paper GT2013-94928.
- Gomes, R. A., and Niehuis, R., 2013, *Film Cooling on Highly Loaded Blades with Main Flow Separation-Part II: Overall Film Cooling Effectiveness*, ASME J. Turbomach., Vol. 135.
- Kusterer, K., Bohn, D., Sugimoto, T., and Tanaka, R., 2007, *Double-Jet Ejection of Cooling Air for Improved Film Cooling*, ASME J. Turbomach., Vol. 129.
- Mathew, S., Ravelli, S.; and bogard, D. G., 2013, *Evaluation of CFD Predictions Using Thermal Field Measurements on a Simulated Film Cooled Turbine Blade Leading Edge*, ASME J. Turbomach., Vol. 135.
- Mhetras, S. Han, J. C., and Rudolph, R., 2012, *Effect of Flow Parameter Variations on Full Coverage Film-Cooling Effectiveness for a Gas Turbine Blade*, ASME J. Turbomach., Vol. 134.
- Naik, S., Krueckels, J, Gritsch, M., and Schnieder, 2014, *Multirow Film Cooling Performances of a High Lift Blade and Vane*, ASME J. Turbomach., Vol. 136.
- Saadati, E., 2009, *Turbulence Modeling*, Sharif University of technology.



- Waye, S. K., Bogard, D. G., 2007, *High-Resolution Film Cooling Effectiveness Comparison of Axial and Compound Angle Holes on the Suction Side of a Turbine Vane*, ASME J. Turbomach., Vol. 129.

## NOMENCLATURE

### Latin Symbols

Symbol	Description	Unit
$C_p$	specific heat	J/ kg.K
$C_f$	turbulent coefficient of skin friction	-
$C$	chord length	mm
$d$	cooling hole diameter	mm
$DR$	density ratio	-
$E$	energy	W
$f$	elliptic relaxation function	-
$H$	span or vane height	mm
$I$	local momentum ratios	-
$k$	turbulence kinetic energy	$m^2/s^2$
$k$	fluid thermal conductivity	W/m.K
$\ell$	the turbulence length scale	mm
$M$	local blowing ratios	-
$Ma$	mach number	-
$\bar{P}$	average pressure	Pa
$P$	hole pitch	mm
$P/d$	pitch ratios	-
$R_{ij}$	reynolds stress tensor	N/m <sup>2</sup>
$Re_c$	reynolds number depending on vane cord length as a characteristic length	-
$Re_d$	reynolds number for the model vane where the characteristic length is the leading edge diameter.	-
$S_h, S_k, S_\epsilon, S_{\bar{v}^2}, S_f$	chemical reaction heat, and any heat source	W
$S$	distance between two stagnation points of vane leading edge.	mm
$s$	distance from stagnation point on vane leading edge downstream along suction side vane surface.	mm
$T_u$	turbulence intensity.	%
$T$	local flow temperature, turbulent time scale.	K
$T_\infty$	mainstream temperature	K
$T_{aw}$	adiabatic wall temperature	K
$T_c$	coolant temperature	K
$TR$	temperature ratio	-
$t$	time	s



$U_\infty$	mean mainstream velocity	m/s
$U_{h,local}$	local hot flow velocity near cooling hole region	m/s
$U_c$	cooling flow velocity at hole exit	m/s
$U_\tau$	shear velocity	m/s
$\vec{V}$	velocity vector	m/s
<b>Greek Symbols</b>		
Symbol	Description	Unit
$\alpha$	inclination angle	degree
$\alpha'$	constant	-
$\beta$	compound or orientation angle	degree
$\beta 1$	vane angle at inlet	degree
$\beta 2$	vane angle at outlet	degree
$\epsilon$	rate of dissipation	m <sup>2</sup> /s <sup>3</sup>
$\eta$	adiabatic film cooling effectiveness	-
$\Delta y$	distance from the wall to the centroid of the first cell	mm
$\mu$	dynamic viscosity	kg/m.s
$\mu_t$	turbulent or eddy viscosity	kg/m.s
$\nu$	kinematic viscosity	m <sup>2</sup> /s
$\rho_h$	hot flow density	kg/m <sup>3</sup>
$\rho_c$	cold flow density	kg/m <sup>3</sup>
$\rho$	density	kg/m <sup>3</sup>
$\tau_w$	wall shear stress	N/m <sup>2</sup>

**Table 1.** Dimensions of actual gas turbine vane (at the mid span) of South Baghdad Power plant and numerical model vane of this study with its initial conditions.

Item	Model vane
Pitch or vane spacing $S$	167mm
Chord length $C$	267mm
Vane angle at inlet $\beta 1$	0 degree
Vane angle at outlet $\beta 2$	76 degree
Inlet uniform velocity $U_\infty$	23.24m/s
Chord Reynolds number $Re_{c,in}$ at inlet boundary	1.49E+05

**Table 2.** Cases studied.

Case no.	M	I	$\alpha$	$\beta$
Case (1)	0.382	0.084	30°	0°
				15°
				30°
Case(2)	0.77	0.34	30°	0°
				15°
				30°
Case(3)	1.14	0.756	30°	0°
				15°
				30°
Case(4)	0.382	0.084	45°	0°
				15°
				30°
				45°
Case(5)	0.77	0.34	45°	0°
				15°
				30°
				45°
Case#6	1.14	0.756	45°	0°
				15°
				30°
				45°

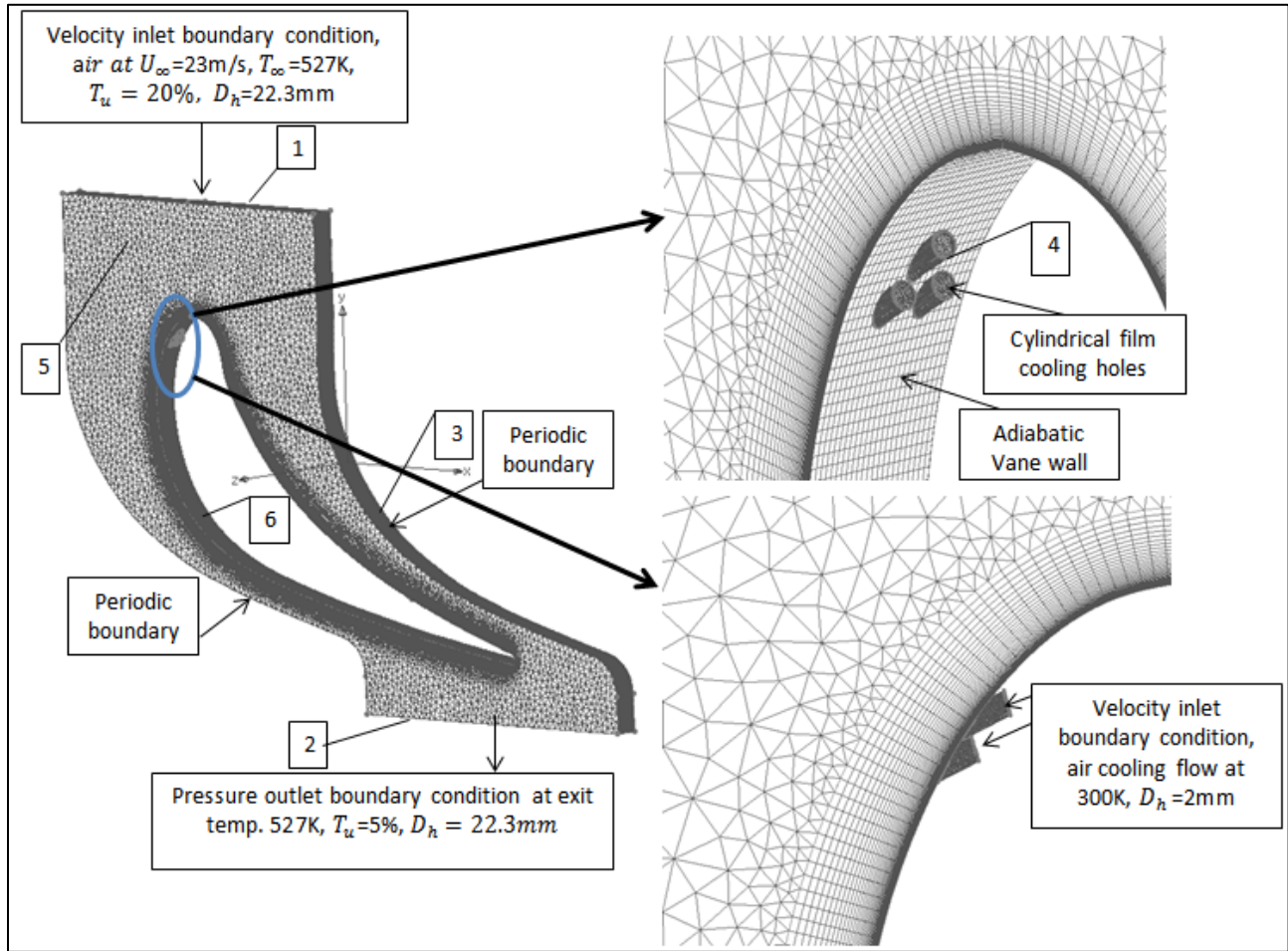


Figure 1. CFD model of vane.

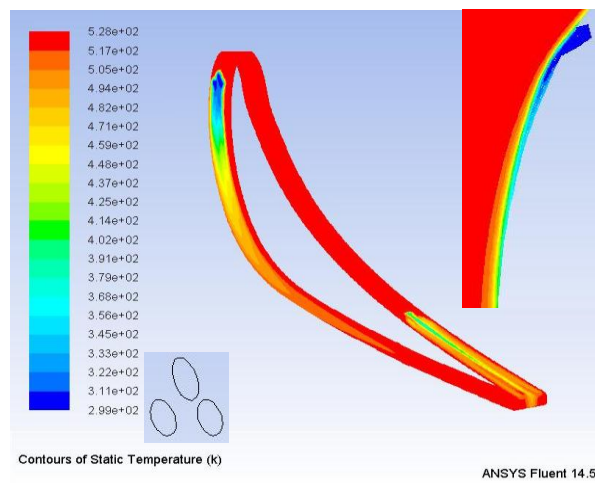


Figure 2. Contours of static temperature K for the vane suction side with staggered film cooling holes. Model for  $M=0.382$ ,  $\alpha=30^\circ$ ,  $P/d=2$ .

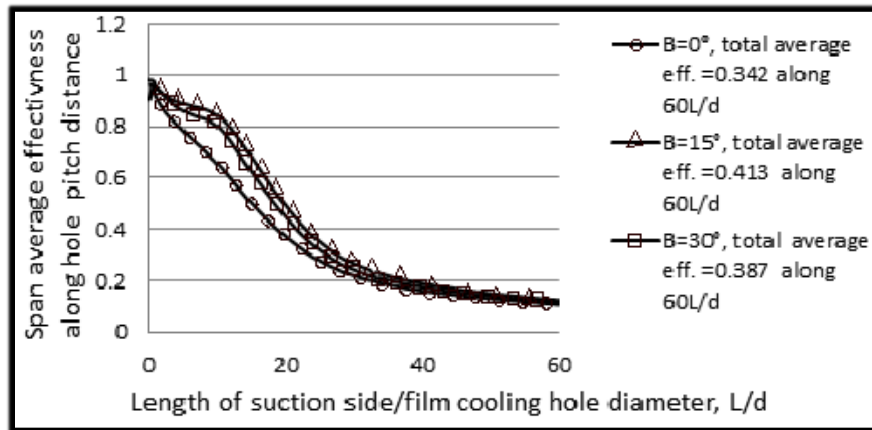


Figure 3. Span average effectiveness for the case 1 at  $\beta = 0^\circ, 15^\circ$  and  $30^\circ$ .

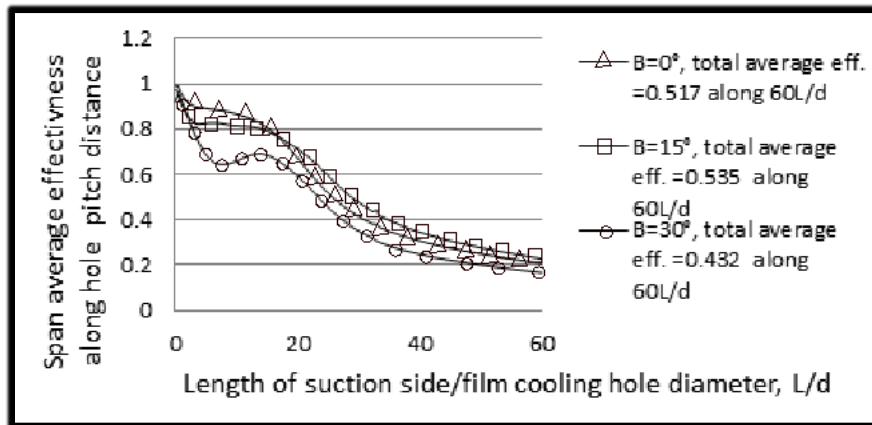


Figure 4. Span average effectiveness for the case 2 at  $\beta = 0^\circ, 15^\circ$  and  $30^\circ$ .

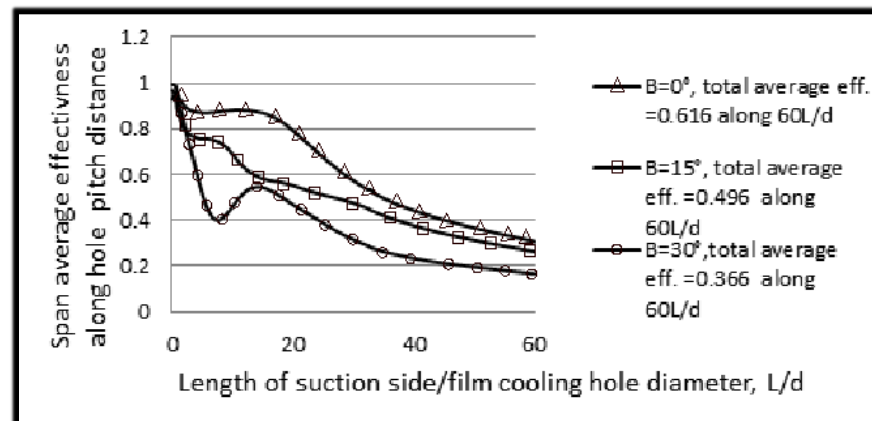


Figure 5. Span average effectiveness for the case 3 at  $\beta = 0^\circ, 15^\circ$  and  $30^\circ$ .

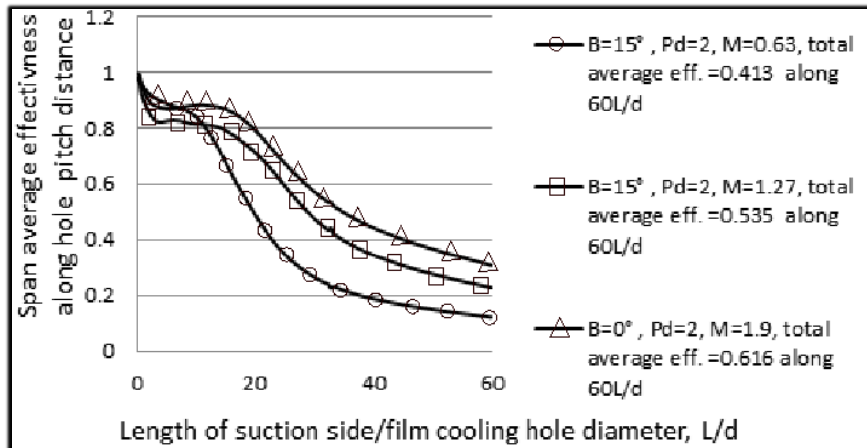


Figure 6. Best span average effectiveness among the cases for  $\alpha=30$ .

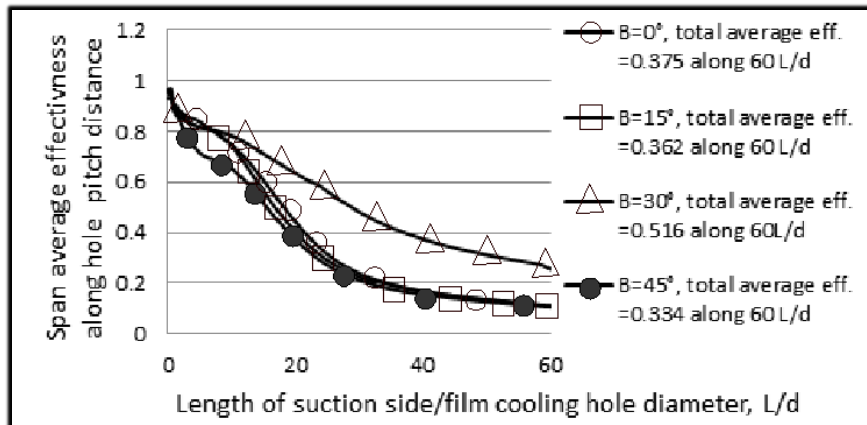


Figure 7. Span average effectiveness for the case 4 at  $\beta= 0^\circ, 15^\circ, 30^\circ,$  and  $45^\circ$ .

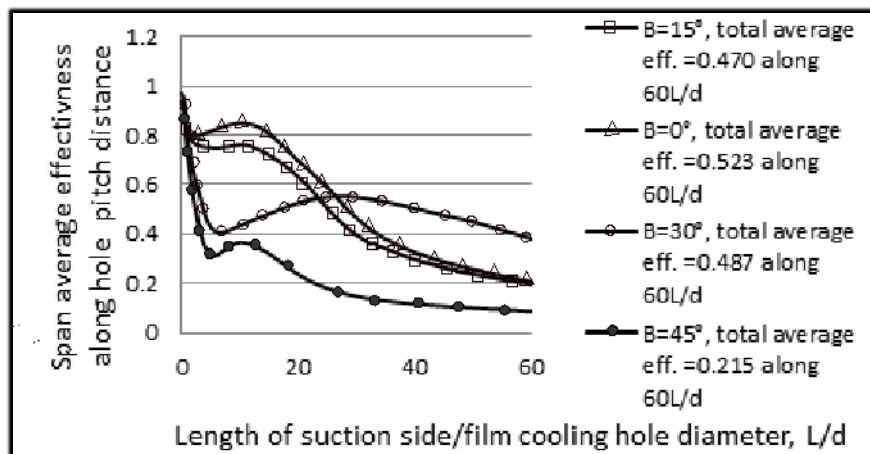


Figure 8. Span average effectiveness for the case 5 at  $\beta= 0^\circ, 15^\circ, 30^\circ,$  and  $45^\circ$ .

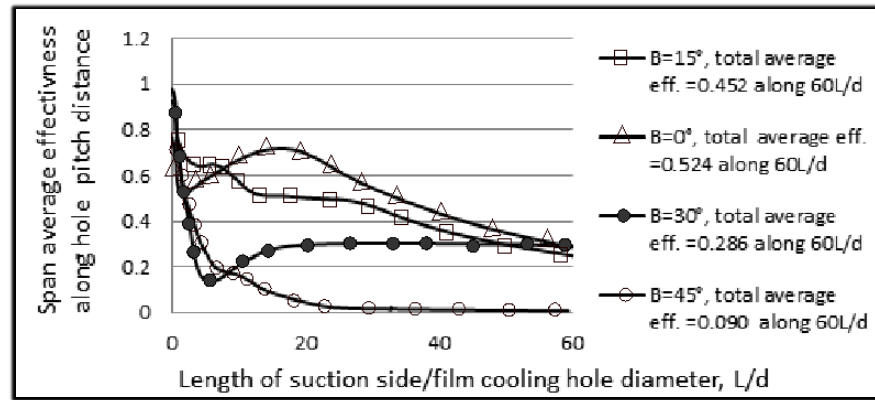


Figure 9. Span average effectiveness for the case 6 at  $\beta=0^\circ, 15^\circ, 30^\circ$ , and  $45^\circ$ .

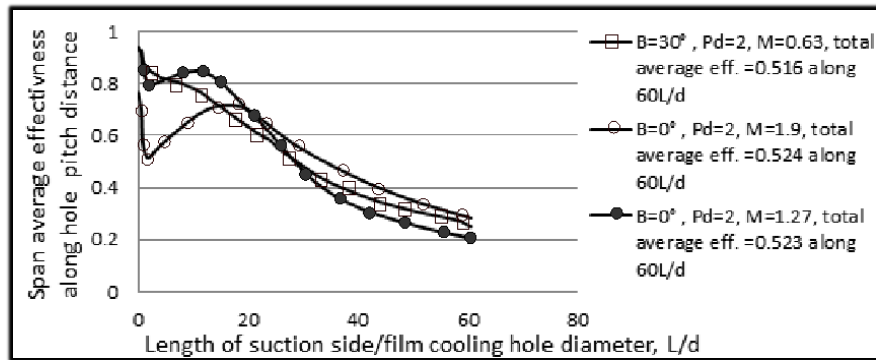


Figure 10. Best span average effectiveness for the cases 4, 5, and 6.

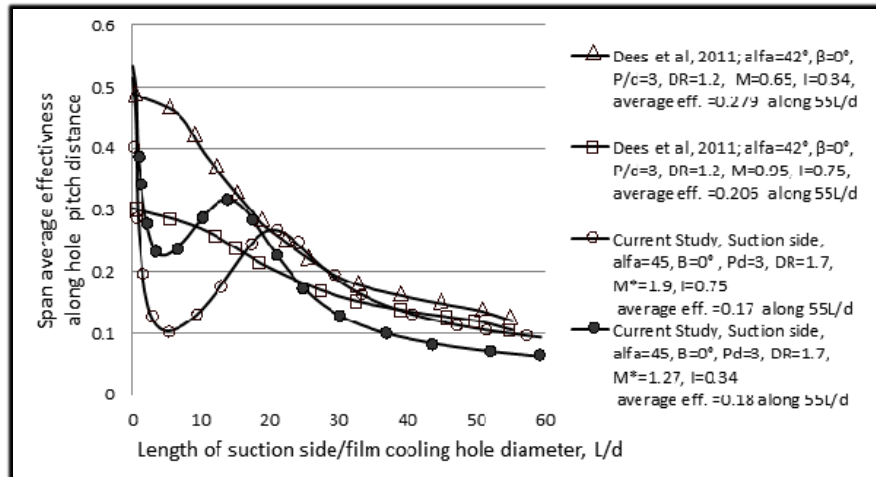


Figure 11. Comparison between results of current study and experimental results of Dees, et al., 2011.